Exploring Large Ductility in Cellulose Nanopaper Combining High Toughness and Strength

Feng Chen, Wenchao Xiang, Daisuke Sawada, Long Bai, Michael Hummel, Herbert Sixta, Tatiana Budtova

Exploring Large Ductility in Cellulose Nanopaper Combining High Toughness and Strength

Feng Chen,[a] Wenchao Xiang,[a] Daisuke Sawada,[a] Long Bai,[a] Michael Hummel,[a] Herbert Sixta,[a] and Tatiana Budtova[a,b]*

[a]Department of Bioproducts and Biosystems, School of Chemical Engineering, Aalto University P.O. Box 16300, FI-00076 Espoo, Finland

[b]Center for Materials Forming-CEMEF, MINES ParisTech, PSL Research University, UMR CNRS 7635, CS 10207, 06904 Sophia Antipolis, France

*Corresponding author:

tatiana.budtova@mines-paristech.fr; tatiana.budtova@aalto.fi

ABSTRACT:

Cellulose nanopaper is a strong lightweight material made from renewable resources with a wide range of potential applications, from membranes to electronic displays. Most studies on nanopaper target high mechanical strength which compromises ductility and toughness. Herein, we demonstrate the fabrication of highly ductile and tough cellulose nanopaper *via* mechanical fibrillation of hemicellulose-rich wood fibers and dispersion of the obtained cellulose nanofibrils (CNFs) in ionic liquid (IL)-water mixture. This treatment allows hemicelluloses swelling leading to dissociation of CNF bundles into highly disordered long flexible fibrils and formation of a nanonetwork as supported by Cryogenic Transmission Electron Microscopy (Cryo-TEM) imaging. Rheology of the suspensions shows a hundredfold increase in storage and loss moduli of CNF-IL-water suspensions as compared to their CNF-water counterparts. The nanopaper prepared by removing the IL-water shows a combination of large elongation up to 35 %, high strength 260 MPa and toughness as high as 51 MJ/m^3 due to efficient interfibrillar slippage and energy dissipation in the highly disordered isotropic structure. This work provides a nanostructure-engineered strategy of making ductile and tough cellulose nanopaper.

KEYWORDS: nanocellulose, ionic liquid, hemicellulose, viscoelastic properties, ductile, mechanical properties

Nature provides us with a variety of nanofibrils that constitute the basic element of many nanostructured biological materials with excellent mechanical properties.[1,2] For example, many natural polymers, such as cellulose in wood,[3] chitin in crustaceans[4] and fibroin in silk[5] form hierarchical structures made of nanofibrils. In general, the mechanical performance of these materials is determined by the mechanical properties of the individual components and their mutual arrangement. Therefore, the understanding and control of structure formation is crucial in the design of materials with desired mechanical properties.

The organization of cellulose nanofibrils (CNFs) in plants and wood represent a classical example of how structural arrangement controls mechanical performance. As an individual component, the elementary CNF with a diameter of 3-4 nm, possesses excellent mechanical properties with Young's modulus of 138 GPa and strength of 2-3 GPa.[6-8] By tuning the orientation of CNFs, both anisotropic and isotropic cellulose films and nanopapers featuring high strength and optical transparency have been designed and tailored through nanostructure engineered strategies, targeting, for example, the substrates for the next-generation of "green" flexible devices[9] and solar cells.[10,11] Anisotropic nanopaper based on oriented CNF (Figure 1a.1) exhibits exceptional strength (> 350 MPa). However, the strain at break is only around 4%, and thus these nanopapers do not offer high mechanical toughness.[12,13] On the contrary, isotropic cellulose nanopaper based on randomly oriented CNFs and its bundles (Figure 1a.2), which are usually obtained by mechanical and/or biochemical fibrillation of wood fibers,[14,15] possess typically a lower strength (< 300 MPa) but a higher fracture strain (up to 10%).[16-19] Like many man-made materials, nanopaper bears a "conflict" between strength and toughness: strong materials are often fragile whereas ductile materials tend to be weak.[20,21] The low ductility of cellulose nanopaper can be a limiting factor for certain applications. For example, petrol-based polyimide films, suggested as a

promising substrate in the field of electronics, have a typical elongation at break of more than 50% and Young's modulus around 3 GPa.[22,23] The challenge is to make cellulose nanopaper which maintains a combination of high strength, ductility, toughness and optical transparency.

Recent investigations reveal that the fracture of cellulose nanopaper under tension involves alignment of CNFs parallel to tension direction and interfibrillar slippage with a cascade of breaking and re-forming hydrogen bonds.[24,25] This leads to the dissipation of a significant amount of energy and contributes to inelastic deformation. In case of anisotropic nanopaper low strain at break and toughness is due to too strong hydrogen bonding between highly ordered nanofibrils, whereas for isotropic nanopaper an increased strain is due to randomly packed CNFs enabling interfibrillar slippage and inelastic deformation. As demonstrated for polymer materials,[26] this is an indication that cellulose nanopaper with highly disordered and long CNFs, like illustrated in Figure 1a.3, may be prone to an effective slippage, significantly contributing to inelastic deformation and causing the stored energy to be released.

It is still challenging to mechanically convert native cellulose fibers into elementary nanofibrils of low polydispersity in diameter while maintaining their length.[27] One of the reasons is that nanofibrils are naturally assembled in bundles stabilized by hydrogen bonds which form inter-fibrillar links. For example, after a mere mechanical disintegration, the resulting CNFs dispersed in water have a very polydisperse fiber diameter due to the presence of CNF bundles, as schematically shown in Figure 1b.[28,29] Although pre-treatments before mechanical disintegration like 2,2,6,6-tetramethylpiperidine-1-oxyl (TEMPO)-mediated oxidation and/or enzymatic hydrolysis help bundles' delamination, these pre-treatments are accompanied by the decrease in fibril length or degree of polymerization of cellulose.[30,31] Therefore, we hypothesize that the preparation of thin and disintegrated nanofibrils of high aspect ratio without compromising their

length would allow for nanopaper with high ductility, that is accessing both high strength and toughness. These highly disordered, long, flexible and entangled CNFs should provide strong networks on the one hand and enable efficient slippage and energy dissipation on the other hand (Figure 1a.3). Furthermore, our goal was to use widely available cellulose fibers from wood and keep the process as simple as possible without using oxidizing chemicals and/or enzymatic treatments. In particular, we purposely kept hemicelluloses, located in-between nanofibrils, for two reasons: firstly, to separate the CNF bundles *via* hemicelluloses swelling and secondly, it was reported that hemicellulose has a softening effect on nanopaper and may facilitate fibril movement under applied stresses thus increasing ductility.[32]

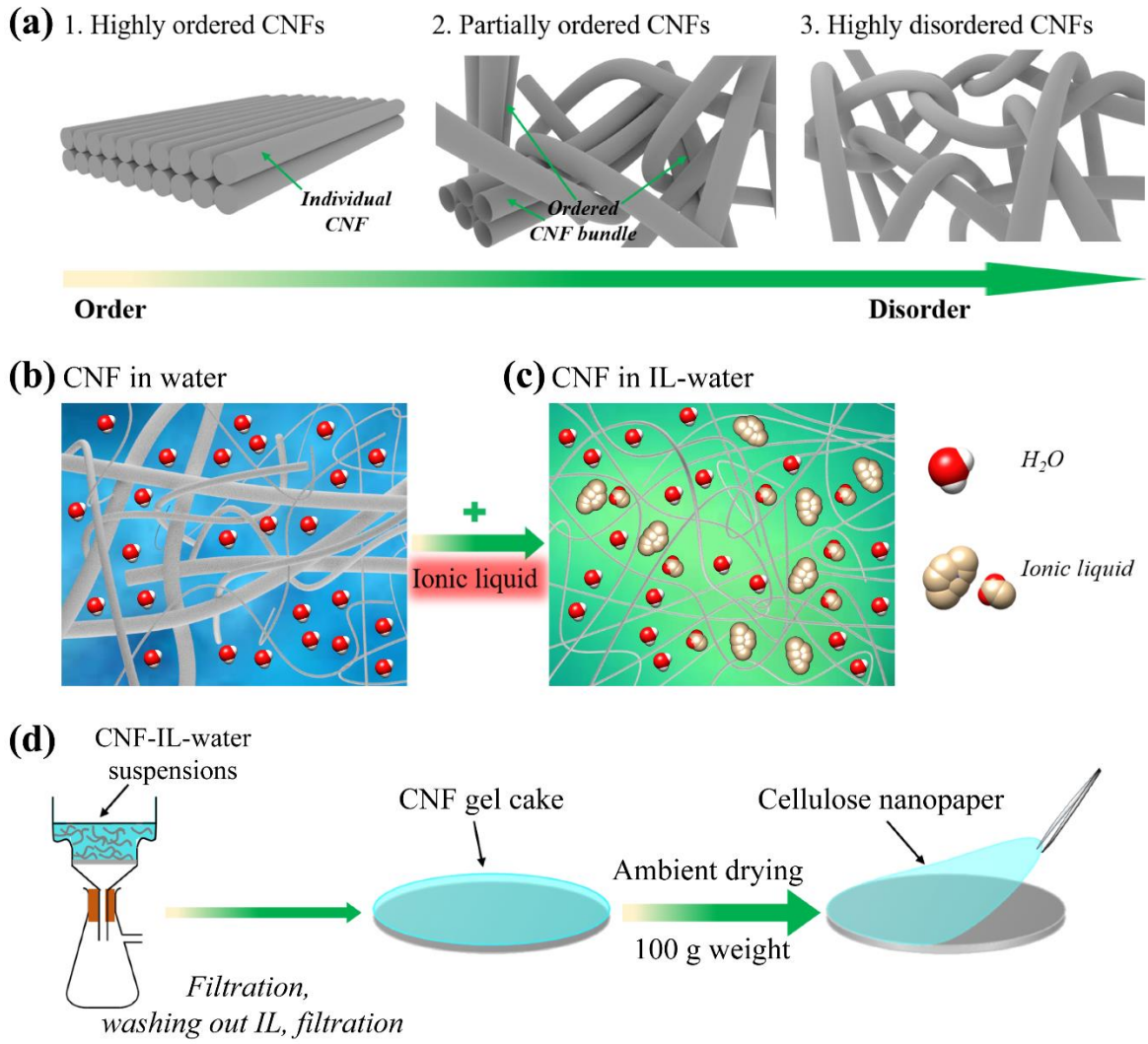

Figure 1. Schematic presentation of the material design concept: a) CNF organization from highly ordered to highly disordered; b) mechanically fibrillated CNFs dispersed in water, showing a mixture of bundles and elementary fibrils; c) CNF dispersed in IL-water with no bundles; d) preparation of cellulose nanopaper from a CNF-IL-water suspension *via* vacuum filtration, washing out IL, filtration and ambient drying.

RESULTS AND DISCUSSION

As a starting material we used wood fibers which were not purified from hemicelluloses, the latter being always present in wood in quantities up to 30%.[32] 0.4 wt.% CNF dispersed in water

was made by passing never-dried fibers through a high-pressure microfluidizer (see details in Experimental Section). The obtained CNF were highly polydisperse in diameter, from few nm to few hundreds nm (Figure S1), and contained around 23 wt.% of hemicelluloses (more details in Table S1 of the Supporting Information).

Next, we used an ionic liquid (IL) 1-ethyl-3-methylimidazolium acetate-water mixture as dispersing medium of CNF (Figure 1c) at IL compositions which are known to neither dissolve cellulose nor hemicellulose.[33,34] X%CNF-Y%IL-W suspensions of various CNF and IL concentrations were prepared from the starting 0.4 wt.% CNF-water stock suspension. The concentration of IL (Y%) was varied from 5 to 50 wt.% and of CNF (X%) from 0.34 to 0.15 wt.%. Reference samples X%CNF-water were made by simple dilution with water of the stock suspension to get the same CNF concentrations as in X%CNF-Y%IL-W.

Nanopapers were prepared from the suspensions by vacuum filtration, removing IL by "washing" with water, further filtration and drying in ambient conditions (Figure 1d and details in Experimental section); the samples are labelled CNF-Y. The details on nomenclature and concentrations of all components in suspensions and corresponding nanopapers are in Table S2.

The analysis of the composition and crystallinity of the initial CNF (after mechanical disintegration) and of the nanopapers showed that hemicelluloses indeed remained in the system after washing out the IL (Table S1). Cellulose was not dissolved either since there was no change in the type of cellulose crystalline phase and degree of crystallinity within the experimental errors (see Figure S2 and Table S1). Note that 50% IL-water was used only as a limiting case to demonstrate that no hemicellulose and cellulose was dissolved even at this high IL concentration; we did not make nanopaper using this IL-water mixture.

Let us first examine the result of the dispersion of CNF bundles in IL-water. We assume that due to the presence of ionic liquid, hemicelluloses located in-between nanofibrils, is swelling and pushing them apart. Consequently, bundles are separated into thinner entities (Figure 1c). As dispersion of the initial CNF in IL-water was performed *via* mild magnetic stirring, no breakage in fibrils' length occurred. The successful delamination of CNF bundles after the treatment with IL was monitored by cryo-TEM. First, to decrease the CNF polydispersity and better visualize the influence of the treatment with ionic liquid, only large bundles were selected by successive centrifugation, discarding the finest fibrils and then the medium fibrils,[28] see details in Figure S3. The suspension of the as-prepared fractionated large bundles was then diluted either with IL-water to CNF-15%IL-water or with water to match the same CNF concentration. CNF dispersed in water (Figure 2a) contains mainly bundles of fibrils with diameter up to hundred nanometers, as also shown by AFM for the initial 0.4%CNF-water suspension (Figure S1). In the presence of 15 wt.% IL, CNF bundles are separated into thinner ones, and even individual elementary nanofibrils can be observed (Figure 2b). The distribution of CNF diameter before and after the treatment with IL is presented in Figure S4, it shows a significant shift of CNF diameter towards lower values. Literature already reported that the presence of hemicelluloses eases the fibrillation of wood fibers into CNF and also prevents nanofibrils agglomeration.[35] Our approach is in-line with the reported role of hemicellulose which, in our case, facilitates disintegration of CNF bundles in the presence of low-concentrated ionic liquid.

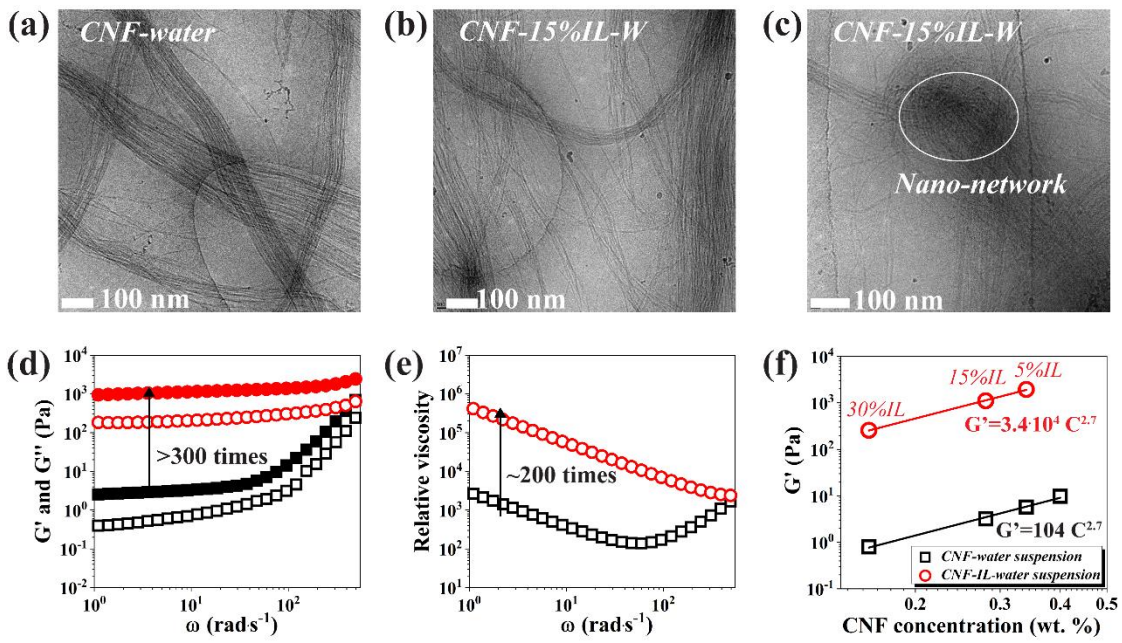

Figure 2. Cryo-TEM (a-c) and viscoelastic properties (d-f) of CNF dispersed in water and in IL-water mixture: a) CNF dispersed in water; b) and c) CNF dispersed in 15%IL-water; d) elastic (G', filled symbols) and viscous (G", open symbols) moduli of 0.28%CNF-water (black squares) and of 0.28%CNF-15%IL-W suspensions (red circles); e) relative viscosity of the same suspensions; f) elastic moduli of CNF-water and CNF-IL-water suspensions as a function of CNF concentration at ω = 7.2 rad/s.

Driven by the observation of this nano-network, we used dynamic rheology to probe the viscoelastic properties of CNF-IL-water suspensions. Figure 2d shows an example of the frequency dependence of elastic (G') and viscous (G") moduli of 0.28% CNF dispersed in 15% IL-water and in water, the examples for other CNF concentrations are given in Figure S4. All suspensions show gel-like behavior with G' being about one order of magnitude higher than the corresponding G", typical for CNF suspensions.[36,37] There is a significant difference between IL-water-based and pure aqueous suspensions: the moduli of 0.28%CNF-15%IL-W suspension are

more than 300 times higher than their corresponding values without ionic liquid. In addition, the frequency-independent region of G' and G" of 0.28%CNF-15%IL-W suspension is much wider than that of 0.28%CNF-water, which is also an indication of a stronger gel. Similar results were recorded for all the prepared CNF suspensions of other concentrations (Figure S5). At high frequencies, CNF-water suspension undergoes a partial phase separation reflected by both moduli increase with frequency increase,[38] which is much less pronounced in the case of CNF-IL-water suspension. The complex viscosity of CNF-IL-water suspensions is also much higher than that of the corresponding CNF-water suspensions, see Figure S6. The viscosity of the dispersing medium itself (Figure S7) does not play a significant role here: Figure 2e demonstrates that relative viscosity of 0.28%CNF-15%-IL is 200 times higher than that of 0.28%CNF-water suspension. This strong increase in viscoelastic behaviour of CNF-IL-water suspensions supports our hypothesis on ionic liquid induced hemicelluloses swelling in CNF bundles inducing their delamination into thinner ones. Thinner dispersed entities are more flexible and form a highly entangled elastic network (Figure 2b, c).

The storage modulus at plateau region of CNF-water and CNF-IL-water suspensions was plotted as a function of CNF concentration *C* (Figure 2f), and each dependence was approximated with the power law used for viscoelastic polymer solutions and also proposed for CNF suspensions:[39,40]

$$G' = KC^{\alpha} \quad (1)$$

where α is a parameter related to network structure,[41] and *K* is a constant proportional to the fiber elastic modulus E_0 and square of fiber aspect ratio.[39,42] In both dispersing media (water and IL-water), *G'* shows a power-law dependence on the CNF concentration with the exponent α equal to 2.7. A slightly higher value (α = 3) was reported for CNF obtained *via* mechanical and enzymatic

treatment,[15] slightly lower values ($\alpha = 2.4$) for carboxymethylated CNF[41] and $\alpha = 2.25$ was reported for macro- and nanocellulose which is matching the theoretical prediction for classical semi-dilute polymer solutions.[39] The constant K of CNF-water suspensions is in the same range as reported previously for CNF dispersed in water, from few tens to a thousand. [39,41] K of the CNF-IL-water suspension is more than 300 times higher than that of their pure aqueous counterparts. The pronounced difference in K value is attributed to the delamination of CNF bundles leading to the decrease in the bundle's diameter while keeping its length: as a consequence, the aspect ratio increases and so does the Young's modulus of the network "building block fiber" as the modulus of an elementary CNF fibril should logically be higher than that of a bundle of nanofibrils assembled together. The latter is known, for example, for natural fibers such as flax, with Young's modulus of bundles' being around 30 GPa while elementary fibers are of higher modulus, around 50 – 70 GPa.[43,44]

The CNF suspensions were then converted into isotropic nanopaper *via* filtration, washing with water to remove the ionic liquid, further filtration and drying. The latter induced shrinkage leading to a decrease of the sample dimensions in longitudinal direction and increase in thickness (Figure S8). We hypothesize that the long and flexible nanofibrils adopt an "accordion"-like structure during drying, which can be a potential cause for the pronounced high elongation under tension due to the nanofibrils gradual unfolding. The nanopaper density decreases from 1.26 to 0.99 g/cm^3 with the increase of IL concentration in the initial dispersing medium from 0 to 15%, respectively. Further increase in IL concentration does not affect the nanopaper density within experimental errors (Table S3). Consequently, nanopaper porosity strongly increases from about 13 to 32 % for the dispersing medium with 0 to 15% IL and then remains around 30% for 30% IL (Table S3).

The potential use of cellulose nanopaper in optoelectronic devices requires high transparency and, in the cases of solar cells, also high haze.[45] Images of the reference nanopaper CNF and CNF15, their optical properties and surface morphology are shown in Figure 3; the properties of other nanopapers are shown in Table S3. Both CNF and CNF15 are highly transparent with no visual difference (Figure 3 a and b), and optical transmittance at wavelength 550 nm is 86.7% and 86.2%, respectively (Figure 3c); similar transmittance was recorded for the other nanopapers (Table S3). Despite the increase in nanopaper porosity with the increase of the IL concentration in the initial dispersing medium, the transparency in the spectral range of visible light remains high (Figure S9 and Table S3) which indicates that pores are below few hundreds nm.

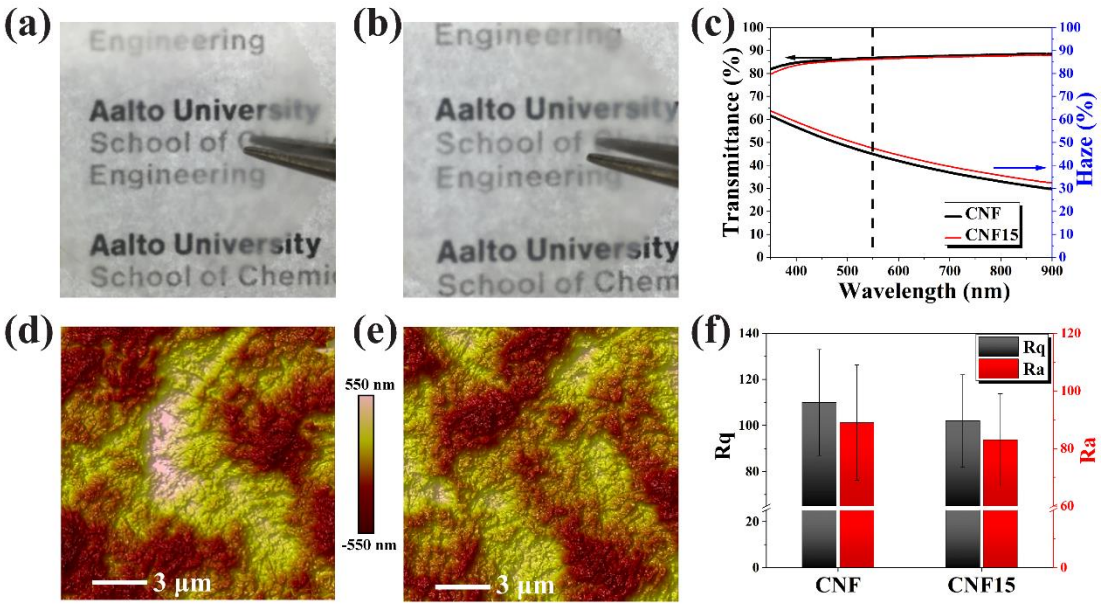

Figure 3. Optical properties and surface morphology of nanopaper: a) and b) digital images of nanopaper CNF and CNF15, respectively; c) optical transmittance and haze of nanopaper CNF and CNF15; d) and e) AFM images of CNF and CNF15 nanopaper, respectively; f) surface roughness values Rq and Ra of nanopaper CNF and CNF15.

For all nanopapers obtained in this work, the optical haze varies from 60 to 30% with the increase of wavelength, and it is slightly higher for the nanopaper from CNF-IL-water suspensions as compared to that from CNF-water (Figure 3c, Figure S9 and Table S3). For example, the haze is 47.5% (nanopaper CNF15) *vs* 44.9% (nanopaper CNF) at wavelength of 550 nm. Usually, a rougher surface contributes to an increased haze.[46] However, AFM results (Figure 3d and e) reveal that nanopaper CNF15, as well as other nanopapers (Table S3), display a smoother surface as compared to nanopaper CNF, which is further supported by roughness values Ra and Rq (Figure 3f and Table S3). The increased haze might derive from the porosity of ionic liquid treated CNF due to folded nanofibrils. A high haze around 50-60% was also obtained for nanopaper from TEMPO-oxidized CNF which is a positive effect in applications such as solar cells, as haze increases light scattering and absorption.[11]

The tensile properties of nanopapers are presented in Figure 4a, b. Stress–strain curves for nanopaper CNF and CNF15 are shown in Figure 4a (three tests per formulation are given as an example to demonstrate reproducibility). CNF15 exhibits an extraordinary combination of large ductility, up to 35%, and high tensile strength, up to 260 MPa. Such high elongation at break coupled with high strength has – to the best of our knowledge – never been reported before for CNF nanopaper. The mean values of elongation and tensile strength of nanopaper CNF15 are much higher than their corresponding values of the reference nanopaper CNF (Figure 4b). Young's modulus of CNF15 shows 30% decrease as compared to that of the reference nanopaper. The properties of other nanopapers, CNF5 and CNF30, are presented in Table S3, all showing high ductility and tensile strength with Young's modulus similar to that of CNF15.

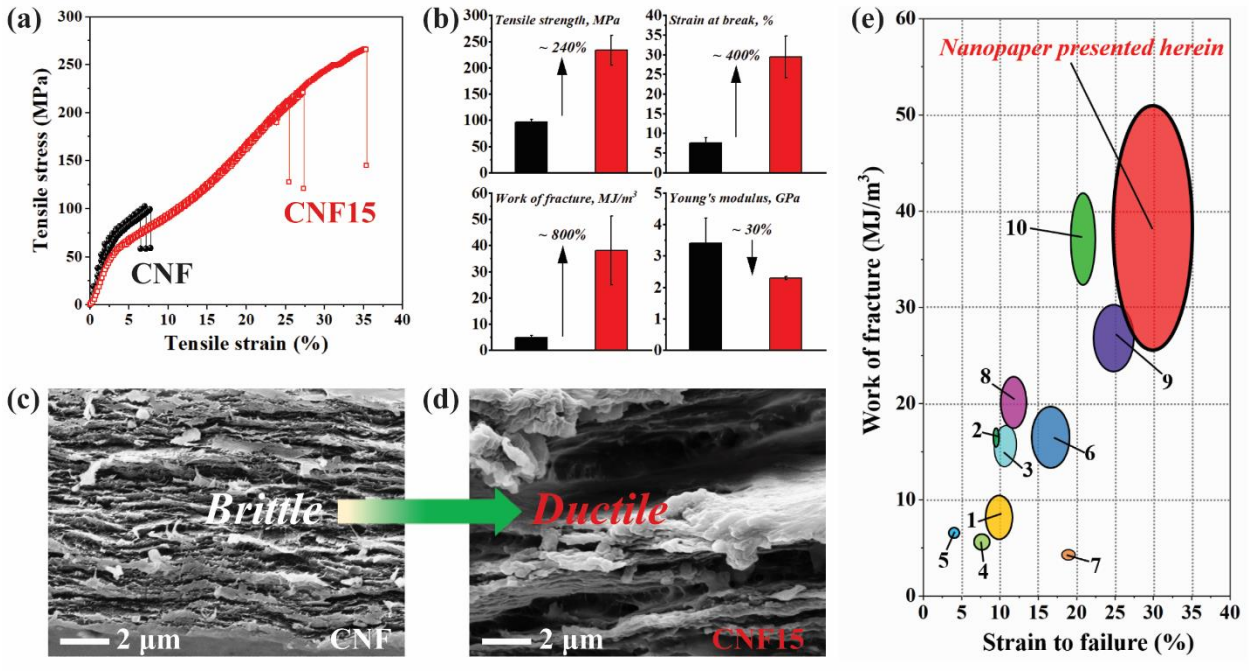

Figure 4. Mechanical properties of nanopaper: a) representative stress-strain curves for nanopaper CNF and CNF15; b) comparison of the mechanical characteristics of nanopaper CNF (black bars) and CNF15 (red bars); c) and d) SEM images of the fractured nanopaper CNF and CNF15, respectively; e) Ashby plot comparing the results obtained in this work with those known from literature for similar systems: 1) isotropic nanopaper from mechanically fibrillated CNF, hot-pressing drying,[56] 2) isotropic nanopaper from TEMPO-oxidized CNF,[25] 3) isotropic nanopaper from enzymatically hydrolyzed CNF,[24] 4) isotropic nanopaper from bacterial cellulose,[57] 5) anisotropic nanopaper from wood *via* delignification and mechanical pressing,[12] 6) isotropic nanopaper from mechanically fibrillated CNF containing 10 wt.% colloidal lignin particles,[56] 7) isotropic nanopaper from TEMPO-oxidized CNF with 50 wt.% vitrimer nanoparticles,[47] 8) isotropic nanopaper from mechanically fibrillated CNF after IL welding,[48] 9) isotropic nanopaper from enzymatically hydrolyzed CNF with 56 vol. % hydroxyethylcellulose,[52] 10) isotropic nanopaper from TEMPO-oxidized CNF with tetrahexyl ammonium as counterion.[49]

The large increase in the ductility of nanopaper CNF15 does not compromise its tensile strength. As a result, the toughness, expressed as a work of fracture, is 38.1 ± 13.1 MJ/m^3 for CNF15, which is a very high value for unmodified nanocellulose based materials.[12,24,25,47,48] To the best of our knowledge, only one cellulose-based nanopaper, with incorporated tetrahexyl ammonium ions (THA^+), had a comparable high toughness 38 MJ/m^3, strain at break of 21% and tensile strength of 272 MPa.[49]

Several factors should be considered in order to interpret the mechanical properties of the obtained nanopapers. Under tension, CNF itself does not show plasticity.[24,50,51] Inter- and intra-fibrils' hydrogen bonds are breaking and reforming during fibrils slippage, the latter "helped" by the presence of hemicelluloses which may act as "lubricant". The fact that CNF are highly disordered also contributed to the decrease in interfibrillar bonding and thus to the efficient sliding. This ease of interfibrillar sliding of entangled CNF allows reaching high elongation at break without losing tensile strength. The increased porosity of nanopapers is also important: pores act as energy dissipators under applied tension. Both factors, slippage and porosity, lead to high ductility and strength but lower modulus. Shrinkage under drying may play an important role as well. If nanofibrils are folding under drying, they unfold under tension and align in the stress direction leading to strain hardening. A slight increase of the slope of the tensile curves (Figure 4a) may be an indication of strain hardening stage. Similar phenomenon was also observed for nanopaper in previous studies[9,49] and indicates an enhanced interfibrillar bonding under tension, confirming the alignment of nanofibrils under deformation. In our work, all factors leading to large ductility and high toughness come together. The fibrils' length remains intact during the delamination of the initial CNF bundles in the IL-water mixture, and a network of long and highly

entangled nanofibrils is formed; CNF folding gives rise to small pores and the preserved hemicelluloses lead to better stress transfer between fibrils under deformation.

The morphology of the fractured surfaces after tensile failure of nanopaper CNF15 and of reference nanopaper CNF is compared in Figure 4c and d, respectively. The laminated nature of the reference sample (Figure 4c) is typical for cellulose nanopaper and is attributed to the flocculation of CNF at a high concentration during filtration,[24,52] confirming a brittle fracture without any fibril pull-outs. The fractured surface of nanopaper CNF15 is extremely bumpy with many microvoids and pull-outs of the mesoscale layers (Figure 4d), similar to ductile nanopapers and their polymer composites.[49,53] This resembles a brittle-to-ductile transition reminiscent of the toughening mechanisms occurring in some thermoplastics and being a sign of excellent energy dissipation.[54]

Literature reports the highest strength for anisotropic nanopapers around 350 MPa. However, those nanopapers suffered from low strain at break (4%), resulting in moderate toughness values (7.38 MJ/m^3).[12] Usually with strength around and above 200 MPa the strain at break of an isotropic nanopaper is 4-7% with maximum values reaching 10 – 12%.[12,17-19,24,25,47,48] As demonstrated in ref.[24], the work at fracture of nanopaper prepared from enzymatically and mechanically disintegrated softwood dissolving pulp was increasing with the increase of cellulose molecular weight, reaching a maximum of 15.1 MJ/m^3, and decreasing with porosity increase; however, hemicellulose content in those pulps was not the same.[24] The decreased work of fracture with porosity increase was mainly due to the decrease in tensile strength while the strain at break did not vary. On the contrary, strain at break was significantly increasing with porosity increase for nanopaper made from either TEMPO- or enzymatically pre-treated and mechanically fibrillated softwood sulfite pulp and dried either with supercritical CO_2 or freeze-dried from butanol.[55] We

compared the mechanical properties of nanopaper CNF15 with the previously reported strong cellulose nanopapers using an Ashby plot (Figure 4e); the values are given in Table S4. The combination of toughness and ductility puts our nanopaper in the top right region, surpassing most of nanopapers reported so far. The modulus is low but acceptable in the applications when a strong material is not the target.

Ionic liquids are still expensive commodities and their recycling has been challenging in cases where very low water contents have to be reached or solubilized biomaterial need to be removed. In this study, however, neither of those challenges were present. In general, materials involving ionic liquids offer high-end applications in photonics, optics, and other areas.[61-65] The presented strategy allows overcoming a general "conflict" between strength and toughness, in particular, for cellulose-based material. The next challenge is to test if the use of other cellulose solvents below their dissolution limit could lead to a similar result.

CONCLUSIONS

We proposed a strategy for the fabrication of highly ductile unmodified cellulose nanopaper which combines high strength and toughness. We benefitted from the presence of hemicelluloses in CNF and used a simple mixing with IL-water followed by filtration and drying. The approach is based on the swelling of hemicelluloses in IL-water mixture at a low IL concentration below the dissolution limit of cellulose and hemicellulose. It allows delamination of thick CNF bundles into thinner ones and results in a strong nano-network of entangled fibrils on the one hand, and efficient interfibrillar slippage and energy dissipation in nanopaper on the other hand. We suggest that porosity created due to nanofibrils folding during drying and unfolding under tension plays an important role in the mechanical properties of nanopaper. The combination of high ductility,

strength, transparency and toughness allows the potential use of cellulose nanopaper as sustainable and biodegradable supports for various applications, for example, in flexible electronics.

EXPERIMENTAL SECTION

Materials. CNF dispersed in water at a concentration of 1.82 wt. % were prepared by passing never-dried, bleached birch pulp (kindly provided by UPM from a Finnish pulp mill) six times through a chamber pair (200 μm and 100 μm) arranged in series in a high-pressure microfluidization (Microfluidics Crop., USA), under a pressure of 2000 bar. The 0.4 wt. % CNF suspension was obtained by dilution with milli-Q water and magnetically stirred for 12 h before using; this suspension was used as the starting batch for further preparations. 1-Ethyl-3-methylimidazolium acetate ([EMIM][OAc], purity >95%) was purchased from IoLiTec and used as received, it is fully miscible with water.[58] The initial moisture content in [EMIM][OAc] was 0.27 wt.% as determined by Karl-Fischer titration. The milli-Q® water was used throughout the experiments.

Preparation of CNF-IL-water suspensions. The starting CNF suspension (0.4 wt.%) was diluted using either 50 wt.% IL-50 wt.% water or 80 wt.% IL-20 wt.% water under magnetic stirring at around 700 rpm for 5 min. Reference suspensions of CNF-water (without ionic liquid) with the same corresponding CNF concentrations were prepared by diluting the starting 0.4 wt.% suspension with water (see Table S1). Fresh suspensions were used to produce nanopaper and for the rheological study.

Preparation of CNF nanopaper. 1) Nanopaper from CNF-water suspensions. CNF-water suspension (0.4 wt.%) was low vacuum filtered on a hydrophilic polyvinylidene fluoride filter membrane (0.22 μm, GVWP, Millipore) until a wet gel cake was formed and no vibration of a

water layer was observed when the filtering apparatus was sharply tapped. The filtration step was completed typically in 10 min. Then a second filter membrane was placed on top of the gel cake, and the whole assembly was dried for 3 days at 25 °C and 50% RH under a 100 g weight. Samples were stored at 25 °C and 50% RH.

2) Nanopaper from CNF-IL-water suspensions. Nanopapers from CNF-IL-water suspensions were produced as described above but the gel cake was washed with water under vacuum filtration for 30 min to remove IL, then filtered to remove water and dried as above. The IL-water mixture may be then collected and re-used, after adjusting the IL concentration, for the subsequent preparations of nanopaper.

The moisture content for all produced nanopaper was within 5% - 7% as determined by vacuum oven drying. The obtained moisture values were in-line with what was reported for a hemicellulose containing nanopaper (about 6% at 50% RH).[35]

The nitrogen content in nanopapers from CNF-IL-water suspensions was determined by elemental analysis. The amount of nitrogen was around 0.1 wt.% which corresponds to around 0.64 wt.% of [EMIM][OAc].

Carbohydrate analysis. The carbohydrate composition of nanopapers was determined by quantitative saccharification upon acid hydrolysis according to NREL/TP-510-42618 norm. Monosaccharides (glucose, xylose and mannose) were quantified by high-performance anion-exchange chromatography equipped with pulse amperometric detection (HPAEC-PAD) and a Dionex ICS-3000 system (Sunnyvale, CA, USA).

X-ray diffraction (XRD). XRD data were collected in the transmission mode setting of an X-ray instrument, SmartLab (RIGAKU), operated at 45 mA and 200 kV. The nanopaper was fixed on a sample holder perpendicular to incident X-ray and the scans were performed in the 2θ range

from 5° to 60° by θ/2θ mode. Background intensity profile without sample was collected in the same conditions, and it was subtracted from the obtained data. Crystallinity was estimated with the Segal method using the intensity of crystal plane (I_{200}) at 2θ = 22.7° and of amorphous parts ($I_{amorphous}$) at 2θ = 18°:

$$CRI = 100 \times \left(\frac{I_{200} - I_{amorphous}}{I_{200}}\right) \quad (2)$$

Cryogenic Transmission Electron Microscopy (Cryo-TEM). 1) Samples preparation for imaging. The initial CNF suspension underwent successive centrifugation using the same procedure as described by Toivonen *et al.*.[28] The goal was to decrease the CNF polydispersity and better visualize the influence of the treatment with ionic liquid. Three successive centrifugations were performed to first separate and discard the finest fibrils, then the medium fibrils and finally to keep the large fibrils only, see Figure S3. The suspension of the large fibrils was then diluted with IL-water mixture to obtain CNF-15%-IL, and with the same amount of water to obtain the reference suspension (CNF-15%-W), which were used to prepare vitrified samples. 2) Cryo-TEM imaging of samples. 3 µL of CNF-15%-IL or CNF-15%-W was placed onto a carbon copper grids (200 mesh, Science Services), from where most of the samples were blotted with a filter paper under 100% humidity, leaving a thin layer of sample over the grids. The specimens were shock-vitrified by fast immersion into liquid ethane-propane mixture at around -180 °C inside a FEI Vitrobot (Zeiss Cryobox, Zeiss NTS GmbH). The vitrified samples were then cryo-transferred to the Cryo-TEM (JEOL 3200FSC Cryo-TEM) operated at 300 kV in bright field mode. The specimens' temperature was kept at - 183 °C. The imaging was carried out with an Omega-type Zero-loss energy filter and acquired with Gatan Ultrascan 4000 CCD camera.

Rheological measurements. The rheological properties of CNF-water and CNF-IL-water suspensions were studied using an Anton Paar MCR 302 rheometer equipped with cone-plate

geometry (cone angle 1°; 50 mm plate diameter) at 25 °C. Strain sweep experiments were conducted within a strain range from 0.01% to 100% at a fixed frequency of 1 Hz in order to determine the linear viscoelastic region which was up to 10% strain. Frequency sweep measurements were carried out at angular frequency range from 0.1 to 1000 rad/s at a strain of 1%.

Atomic Force Microscopy (AFM). AFM (MultiMode 8 Scanning Probe Microscope, Bruker AXS Inc.) was used to analyze the initial CNF dispersed in water and the surface morphology and roughness of the obtained nanopapers. The initial CNF suspension was diluted to 0.01 wt.% and spin-coated onto polyethyleneimine-coated mica. The nanofibril-coated substrate was dried overnight at room temperature before imaging. The AFM scans (3 μm × 3 μm for CNF-water suspension and 15 μm × 15 μm for nanopaper surface) were collected under tapping mode in air with silicon cantilevers (NSC15/AIBS, MicroMasch). In the case of nanopapers, ten different areas were scanned to obtain mean value of roughness Rq (the root mean square average of height deviation taken from the mean image data plane) and Ra (the arithmetic average of the absolute values of the surface height deviations measured from the mean plane).

Scanning Electron Microscopy (SEM). The cryo-fracture and tensile-fracture cross-sections of the nanopapers were observed by using a scanning electron microscope (Zeiss Sigma VP FE-SEM) at an accelerating voltage of 4 kV. Prior to examination, the fracture cross-sections of the specimens were coated with a thin layer of gold.

Density and Porosity. The density of the nanopaper was determined by measuring its weight and dividing it by its volume. The volume was calculated from the thickness of the nanopaper and its area, while the thickness was measured by using L&W Micrometer (Lorentzen & Wettre Products, ABB, Switzerland) with an error of ± 1 μm or 0.1 % of reading whichever is greater.

Porosity was estimated from the density of the nanopaper by taking 1.46 g. cm^{-3} as density of cellulose[59] using the equation:

$$Porosity = \left[1 - \frac{\rho_{nanopaper}}{\rho_{cellulose}}\right] \times 100\% \quad (3)$$

Ultraviolet–Visible Light (UV–vis) Spectroscopy. The optical properties of transmittance and haze of the nanopapers were obtained using a Shimadzu UV-2600 with an ISR-2600 Plus Integrating Sphere Attachment (Shimadzu, Japan.), and the transmittance was measured between 1200 nm and 200 nm. Optical haze was used to quantify the percentage of the forward light scattering as follows:[60]

$$Haze = \left[\frac{T_4}{T_2} - \frac{T_3}{T_1}\right] \times 100\% \quad (4)$$

where T1, T2, T3 and T4 are defined as background checking, total transmitted illumination, beam checking and pure diffusive transmittance, respectively.

Tensile Testing. The mechanical properties were studied by using Instron 4204 Universal Tensile Tester (INSTRON, United Kingdom). More than ten specimens with known thicknesses (20 mm × 4 mm, length and width, respectively) of each formulation were conditioned for 24 hours in a controlled environment of 50 % relative humidity and 23 °C. Sample edges were glued onto a paper frame (leaving a gauge length of 10 mm) to avoid slippage and deformed at a rate of 0.5 mm/min using a 100 N load cell. As no extensometer was used, all values reported were nominal (engineering).

ASSOCIATED CONTENT

Supporting Information Available online at the ACS Publications website: AFM of the initial CNFs; Table of chemical composition and crystallinity of nanopaper before and after treatment with ionic liquid; Table of nomenclature and concentrations of all components in

suspensions and corresponding nanopaper; XRD of CNFs before and after the treatment with ionic liquid; schematic illustration of CNF fractionation by successive centrifugation; Cryo-TEM based CNF diameter distributions before (a) and after (b) the treatment with IL; dynamic rheology of prepared CNF suspensions; digital images and SEM images (Cryo-fractured cross-sections) of the prepared nanopapers; optical transmittance and haze of the prepared nanopapers; Table of physical and mechanical properties of the nanopapers obtained; Table of the mechanical properties of nanopapers shown in Figure 4.

AUTHOR INFORMATION

Corresponding Authors

*Email: tatiana.budtova@mines-paristech.fr; tatiana.budtova@aalto.fi

ORCID ID

Feng Chen: 0000-0002-9867-5633

Wenchao Xiang: 0000-0003-4281-3109

Daisuke Sawada: 0000-0002-5789-2551

Long Bai: 0000-0003-3356-9095

Michael Hummel: 0000-0002-6982-031X

Herbert Sixta: 0000-0002-9884-6885

Tatiana Budtova: 0000-0003-1835-2146

CONFLICT OF INTEREST

The authors declare no competing financial interest.

ACKNOWLEDGMENTS

The financial support from Business Finland (Grant No. 211599), Stora Enso Oyj and UPM-Kymmene Oyj are gratefully acknowledged. Authors wish to thank Separation Research Oy Ab and Fibertus Oy for collaboration. We also acknowledge the provision of facilities and technical support by Aalto University at OtaNano-Nanomicroscopy Center (Aalto-NMC).

REFERENCES

(1) Ling, S.; Kaplan, D. L.; Buehler, M. J. Nanofibrils in Nature and Materials Engineering. *Nat. Rev. Mater.* **2018**, *3*, 1-5.

(2) Martin-Martinez, F. J.; Jin, K.; López, Barreiro, D.; Buehler, M. J. The Rise of Hierarchical Nanostructured Materials from Renewable Sources: Learning from Nature. *ACS Nano* **2008**, *12*, 7425-7433.

(3) Barthelat, F.; Yin, Z.; Buehler, M. J. Structure and Mechanics of Interfaces in Biological Materials. *Nat. Rev. Mater.* **2016**, *1*, 1-16.

(4) Raabe, D.; Sachs, C.; Romano, P. J. A. M. The Crustacean Exoskeleton as an Example of a Structurally and Mechanically Graded Biological Nanocomposite Material. *Acta Mater.* **2005**, *53*, 4281-4292.

(5) Tao, H.; Kaplan, D. L.; Omenetto, F. G. Silk Materials A Road to Sustainable High Technology. *Adv. Mater.* **2012**, *24*, 2824-2837.

(6) Sakurada, I.; Nukushina, Y.; Ito, T. Experimental Determination of the Elastic Modulus of Crystalline Regions in Oriented Polymers. *J. Polym. Sci.* **1962**, *57*, 651-660.

(7) Page, D. H.; El-Hosseiny, F. Mechanical Properties of Single Wood Pulp Fibres. VI. Fibril Angle and the Shape of the Stress-Strain Curve. *Pulp Paper Sci.* **1983**, *9*, 99.

(8) Saito, T.; Kuramae, R.; Wohlert, J.; Berglund, L. A.; Isogai, A. An Ultrastrong Nanofibrillar Biomaterial: The Strength of Single Cellulose Nanofibrils Revealed *via* Sonication-Induced Fragmentation. *Biomacromolecules* **2012**, *14*, 248-253.

(9) Toivonen, M. S.; Kaskela, A.; Rojas, O. J.; Kauppinen, E. I.; Ikkala, O. Ambient-Dried Cellulose Nanofibril Aerogel Membranes with High Tensile Strength and Their Use for Aerosol

Collection and Templates for Transparent, Flexible Devices. *Adv. Funct. Mater.* **2015**, *25*, 6618-26.

(10) Zhu, H.; Fang, Z.; Preston, C.; Li, Y.; Hu, L. Transparent Paper: Fabrications, Properties, and Device Applications. *Energy Environ. Sci.* **2014**, *7*, 269-287.

(11) Fang, Z.; Zhu, H.; Yuan, Y.; Ha, D.; Zhu, S.; Preston, C.; Chen, Q.; Li, Y.; Han, X.; Lee, S.; Chen, G. Novel Nanostructured Paper with Ultrahigh Transparency and Ultrahigh Haze for Solar Cells. *Nano Lett.* **2014**, *14*, 765-73.

(12) Zhu, M.; Wang, Y.; Zhu, S.; Xu, L.; Jia, C.; Dai, J.; Song, J.; Yao, Y.; Wang, Y.; Li, Y.; Henderson, D. Anisotropic, Transparent Films with Aligned Cellulose Nanofibers. *Adv. Mater.* **2017**, *29*, 1606248.

(13) Wang, S.; Li, T.; Chen, C.; Kong, W.; Zhu, S.; Dai, J.; Diaz, A. J.; Hitz, E.; Solares, S. D.; Li, T; Hu, L. Transparent, Anisotropic Biofilm with Aligned Bacterial Cellulose Nanofibers. *Adv. Funct. Mater.* **2018**, *28*, 1707491.

(14) Klemm, D.; Heublein, B.; Fink, H. P.; Bohn, A., Cellulose: Fascinating Biopolymer and Sustainable Raw Material. *Angew. Chem. Int. Ed. Engl.* **2011**, *50*, 5438-3393.

(15) Pääkkö, M.; Ankerfors, M.; Kosonen, H.; Nykänen, A.; Ahola, S.; Österberg, M.; Ruokolainen, J.; Laine, J.; Larsson, P. T.; Ikkala, O.; Lindström, T. Enzymatic Hydrolysis Combined with Mechanical Shearing and High-Pressure Homogenization for Nanoscale Cellulose Fibrils and Strong Gels. *Biomacromolecules* **2007**, *8*,1934-1941.

(16) Nogi, M.; Iwamoto, S.; Nakagaito, A. N.; Yano, H. Optically Transparent Nanofiber Paper. *Adv. Mater.* **2009**, *21*, 1595-1598.

(17) Fukuzumi, H.; Saito, T.; Iwata, T.; Kumamoto, Y.; Isogai, A. Transparent and High Gas Barrier Films of Cellulose Nanofibers Prepared by TEMPO-Mediated Oxidation. *Biomacromolecules* **2009**, *10*, 162-165.

(18) Sehaqui, H.; Liu, A.; Zhou, Q.; Berglund, L. A., Fast Preparation Procedure for Large, Flat Cellulose and Cellulose/Inorganic Nanopaper Structures. *Biomacromolecules* **2010**, *11*, 2195-2198.

(19) Österberg, M.; Vartiainen, J.; Lucenius, J.; Hippi, U.; Seppälä, J.; Serimaa, R.; Laine, J. A Fast Method to Produce Strong NFC Films as a Platform for Barrier and Functional Materials. *ACS Appl. Mater. Interfaces* **2013**, *5*, 4640-4647.

(20) Ritchie, R. O. The Conflicts between Strength and Toughness. *Nat. Mater.* **2011**, *10*, 817-822.

(21) Giesa, T.; Buehler, M. J. Nanoconfinement and the Strength of Biopolymers. *Annu. Rev. Biophys.* **2013**, *42*, 651-673.

(22) Katayama, M.; Hiraishi, K.; Suto, Y.; Okazaki, N; Wang, H. (Nippon Steel and Sumikin Chemical Co Ltd) Display Device, Method for Manufacturing Same, Polyimide Film for Display Device Supporting Bases, and Method for Producing Polyimide Film for Display Device Supporting Bases. U.S. Patent No. 9,403,947. **2016**.

(23) Chang, W. Y.; Fang, T. H.; Lin, Y. C. Physical Characteristics of Polyimide Films for Flexible Sensors. *Appl. Phys. A* **2008**, *92*, 693.

(24) Henriksson, M.; Berglund, L. A.; Isaksson, P.; Lindstrom, T; Nishino, T. Cellulose Nanopaper Structures of High Toughness. *Biomacromolecules* **2008**, *9*, 1579-1585.

(25) Zhu, H.; Zhu, S.; Jia, Z.; Parvinian, S.; Li, Y.; Vaaland, O.; Hu, L.; Li, T. Anomalous Scaling Law of Strength and Toughness of Cellulose Nanopaper. *Proc. Natl. Acad. Sci. U S A* **2015**, *112*, 89718976.

(26) Fava, D.; Fan, Y. S.; Kumacheva, E.; Winnik, M. A.; Shinozaki, D. M. Order *versus* Disorder: Effect of Structure on the Mechanical Properties of Polymer Material. *Macromolecules* **2006**, *39*, 1665-1669.

(27) Saito, T.; Nishiyama, Y.; Putaux, J. L.; Vignon, M.; Isogai, A. Homogeneous Suspensions of Individualized Microfibrils from TEMPO-Catalyzed Oxidation of Native Cellulose. *Biomacromolecules* **2006**, *7*, 1687-1691.

(28) Toivonen, M. S.; Onelli, O. D.; Jacucci, G.; Lovikka, V.; Rojas, O. J.; Ikkala, O.; Vignolini, S. Anomalous-Diffusion-Assisted Brightness in White Cellulose Nanofibril Membranes. *Adv. Mater.* **2018**, *30*, 1704050.

(29) Pöhler, T.; Lappalainen, T.; Tammelin, T.; Eronen, P.; Hiekkataipale, P.; Vehniäinen, A.; Koskinen, T. M. Influence of Fibrillation Method on the Character of Nanofibrillated Cellulose (NFC). In *2010 Intl' Conference on Nanotechnology for the Forest Products Industry*, Espoo, Finland, September 2010; TAPPI Press, pp. 437-458.

(30) Benítez, A. J.; Walther, A. Cellulose Nanofibril Nanopapers and Bioinspired Nanocomposites: A Review to Understand the Mechanical Property Space. *J. Mater. Chem. A* **2017**, *5*, 16003-16024.

(31) Nechyporchuk, O.; Belgacem, M. N.; Bras, J. Production of Cellulose Nanofibrils: A Review of Recent Advances. *Ind. Crop. Prod.* **2016**, *93*, 2-25.

(32) Arola, S.; Malho, J. M.; Laaksonen, P.; Lille, M.; Linder, M. B. The Role of Hemicellulose in Nanofibrillated Cellulose Networks. *Soft Matter* **2013**, *9*, 1319-1326.

(33) Le, K. A.; Sescousse, R.; Budtova, T. Influence of Water on Cellulose-EMIMAc Solution Properties: A Viscometric Study. *Cellulose* **2012**, *19*, 45-54.

(34) Froschauer, C.; Hummel, M.; Iakovlev, M.; Roselli, A.; Schottenberger, H.; Sixta, H. Separation of Hemicellulose and Cellulose from Wood Pulp by Means of Ionic Liquid/Cosolvent Systems. *Biomacromolecules*, **2013**, *14*, 1741-1750.

(35) Galland, S.; Berthold, F.; Prakobna, K.; Berglund, L. A. Holocellulose Nanofibers of High Molar Mass and Small Diameter for High-Strength Nanopaper. *Biomacromolecules* **2015**, *16*, 2427.

(36) Li, M. C.; Wu, Q.; Song, K.; Lee, S.; Qing, Y.; Wu, Y. Cellulose Nanoparticles: Structure–Morphology–Rheology Relationships. *ACS Sustain. Chem. Eng.* **2015**, *3*, 821-832.

(37) Geng, L.; Mittal, N.; Zhan, C.; Ansari, F.; Sharma, P. R.; Peng, X.; Hsiao, B. S.; Söderberg, L. D. Understanding the Mechanistic Behavior of Highly Charged Cellulose Nanofibers in Aqueous Systems. *Macromolecules* **2018**, *51*, 1498-1506.

(38) Charani, P. R.; Dehghani-Firouzabadi, M.; Afra, E.; Shakeri, A. Rheological Characterization of High Concentrated MFC Gel from Kenaf Unbleached Pulp. *Cellulose* **2013**, *20*, 727-740.

(39) Tatsumi, D.; Ishioka, S.; Matsumoto, T. Effect of Fiber Concentration and Axial Ratio on the Rheological Properties of Cellulose Fiber Suspensions. *J. Soc. Rheol. Japan,* **2002**, *30*, 27-32.

(40) MacKintosh, F. C.; Käs, J.; Janmey, P. A. Elasticity of Semiflexible Biopolymer Networks. *Phys. Rev. Lett.* **1995**, *75*, 4425.

(41) Naderi, A.; Lindström, T.; Sundström, J. Carboxymethylated Nanofibrillated Cellulose: Rheological Studies. *Cellulose* **2014**, *21*, 1561-1571.

(42) Bennington, C. P. J.; Kerekes, R. J.; Grace, J. R. The Yield Stress of Fibre Suspensions. *Can. J. Chem. Eng.* **1990**, *68*, 748-757.

(43) Yan, L.; Chouw, N.; Jayaraman, K. Flax Fibre and Its Composites – A Review. *Compos. Part B-Eng.* **2014**, *56*, 296-317.

(44) Charlet, K.; Jernot, J. P.; Gomina, M.; Bizet, L.; Bréard, J. Mechanical Properties of Flax Fibers and of the Derived Unidirectional Composites. *J. Compos. Mater.* **2010**, *44*, 2887-2896.

(45) Chiba, Y.; Islam, A.; Watanabe, Y.; Komiya, R.; Koide, N.; Han, L. Dye-Sensitized Solar Cells with Conversion Efficiency of 11.1%. *Jpn. J. Appl. Phys.* **2006**, *45*, 638.

(46) Johnson, M. B.; Wilkes, G. L.; Sukhadia, A. M.; Rohlfing, D. C. Optical Properties of Blown and Cast Polyethylene Films: Surface *versus* Bulk Structural Considerations. *J. Appl. Polym. Sci.* **2000**, *77*, 2845-2864.

(47) Lossada, F.; Guo, J.; Jiao, D.; Groeer, S.; Bourgeat-Lami, E.; Montarnal, D.; Walther, A. Vitrimer Chemistry Meets Cellulose Nanofibrils: Bioinspired Nanopapers with High Water Resistance and Strong Adhesion. *Biomacromolecules* **2019**, *20*, 1045-1055.

(48) Reyes, G.; Borghei, M.; King, A. W.; Lahti, J.; Rojas, O. J. Solvent Welding and Imprinting Cellulose Nanofiber Films Using Ionic Liquids. *Biomacromolecules* **2019**, *20*, 502-514.

(49) Benítez, A. J.; Walther, A. Counterion Size and Nature Control Structural and Mechanical Response in Cellulose Nanofibril Nanopapers. *Biomacromolecules* **2017**, *18*, 1642-1653.

(50) Tang, H.; Butchosa, N.; Zhou, Q. A Transparent, Hazy, and Strong Macroscopic Ribbon of Oriented Cellulose Nanofibrils Bearing Poly (ethylene Glycol). *Adv. Mater.* **2015**, *27*, 2070-2076.

(51) Ansari, F.; Berglund, L. A. Tensile Properties of Wood Cellulose Nanopaper and Nanocomposite Films. In *Multifunctional Polymeric Nanocomposites Based on Cellulosic Reinforcements*; David. J., Eds.; William Andrew Publishing: Oxford, 2016; pp. 115-130.

(52) Sehaqui, H.; Zhou, Q.; Berglund, L. A. Nanostructured Biocomposites of High Toughness — A Wood Cellulose Nanofiber Network in Ductile Hydroxyethylcellulose Matrix. *Soft Matter* **2011**, *7*, 7342-7350.

(53) Benítez, A. J.; Lossada, F.; Zhu, B.; Rudolph, T.; Walther, A. Understanding Toughness in Bioinspired Cellulose Nanofibril/Polymer Nanocomposites. *Biomacromolecules* **2016**, *17*, 2417-26.

(54) Xu, H.; Xie, L.; Chen, J. B.; Jiang, X.; Hsiao, B. S.; Zhong, G. J.; Fu, Q.; Li, Z. M. Strong and Tough Micro/Nanostructured Poly (lactic Acid) by Mimicking the Multifunctional Hierarchy of Shell. *Mater. Horiz.* **2014**, *1*, 546-552.

(55) Sehaqui, H.; Zhou, Q.; Ikkala, O.; Berglund, L. A. Strong and Tough Cellulose Nanopaper with High Specific Surface Area and Porosity. *Biomacromolecules* **2011**, *12*, 3638-3644.

(56) Farooq, M.; Zou, T.; Riviere, G.; Sipponen, M. H.; Österberg, M. Strong, Ductile, and Waterproof Cellulose Nanofibril Composite Films with Colloidal Lignin Particles. *Biomacromolecules* **2019**, *20*, 693-704.

(57) Lee, K. Y.; Tammelin, T.; Schulfter, K.; Kiiskinen, H.; Samela, J.; Bismarck, A. High Performance Cellulose Nanocomposites: Comparing the Reinforcing Ability of Bacterial Cellulose and Nanofibrillated Cellulose. *ACS Appl. Mater. Interfaces* **2012**, *4*, 4078-4086.

(58) Hall, C. A.; Le, K. A.; Rudaz, C.; Radhi, A.; Lovell, C. S.; Damion, R. A.; Budtova, T.; Ries, M. E. Macroscopic and Microscopic Study of 1-Ethyl-3-Methyl-Imidazolium Acetate-Water Mixtures. *J. Phys. Chem. B* **2012**, *116*, 12810-8.

(59) Sun, C. C. Mechanism of Moisture Induced Variations in True Density and Compaction Properties of Microcrystalline Cellulose. *Int. J. Pharm*. **2008**, *346*, 93-101.

(60) Zhu, H.; Parvinian, S.; Preston, C.; Vaaland, O.; Ruan, Z; Hu, L. Transparent Nanopaper with Tailored Optical Properties. *Nanoscale* **2013**, *5*, 3787-3792.

(61) Meng, X.; Al-Salman, R.; Zhao, J.; Borissenko, N.; Li, Y.; Endres. F. Electrodeposition of 3D Ordered Macroporous Germanium from Ionic Liquids: a Feasible Method to Make Photonic Crystals with a High Dielectric Constant. *Angew. Chem. Int. Ed. Engl.* **2009**, *48*, 2703-7.

(62) Bai, L.; Xie, Z.; Wang, W.; Yuan, C.; Zhao, Y.; Mu, Z.; Zhong, Q.; Gu, Z. Bio-inspired Vapor-Responsive Colloidal Photonic Crystal Patterns by Inkjet Printing. *ACS Nano* **2014**, *8*, 11094-100.

(63) Kim, G. T.; Kennedy, T.; Brandon, M.; Geaney, H.; Ryan, K. M.; Passerini, S, Appetecchi, G. B. Behavior of Germanium and Silicon Nanowire Anodes with Ionic Liquid Electrolytes. *ACS Nano* **2017**, *11*, 5933-43.

(64) Nakashima, T.; Zhu, J.; Qin, M.; Ho, S.; Kotov, N. A. Polyelectrolyte and Carbon Nanotube Multilayers Made from Ionic Liquid Solutions. *Nanoscale* **2010**, *2*, 2084-90.

(65) Zhang, Y.; Cui, B.; Yang, H.; Gao, F.; Parkin, S. S. Ionic Liquid Gate-Induced Modifications of Step Edges at $SrCoO_{2.5}$ Surfaces. *ACS Nano* **2020**.

For the Table of Contents Only

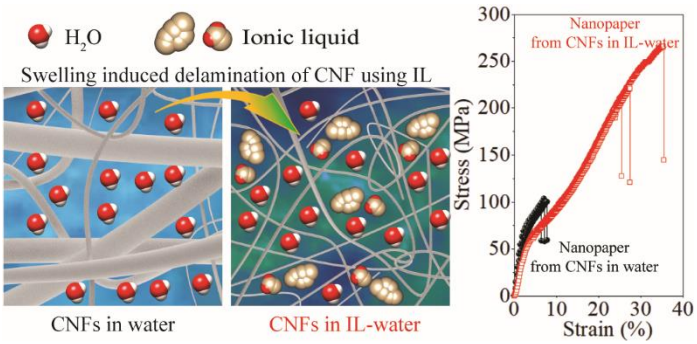

Supporting Information

Exploring Large Ductility in Cellulose Nanopaper Combining High Toughness and Strength

Feng Chen,[a] *Wenchao Xiang,*[a] *Daisuke Sawada,*[a] *Long Bai,*[a] *Michael Hummel,*[a] *Herbert Sixta,*[a] *and Tatiana Budtova**[a,b]

[a] Department of Bioproducts and Biosystems, School of Chemical Engineering, Aalto University P.O. Box 16300, FI-00076 Espoo, Finland

[b] Center for Materials Forming-CEMEF, MINES ParisTech, PSL Research University, UMR CNRS 7635, CS 10207, 06904 Sophia Antipolis, France

*Corresponding author: tatiana.budtova@mines-paristech.fr; tatiana.budtova@aalto.fi

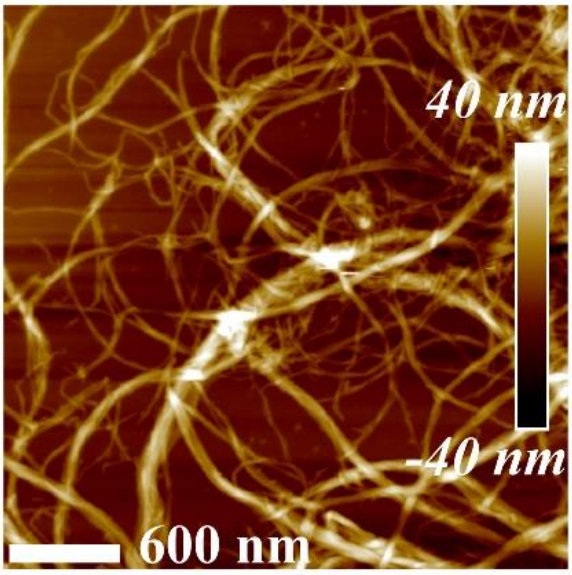

Figure S1. AFM image of the initial CNF-water suspension, before dispersing in ionic liquid

Table S1. Composition and crystallinity of the initial and IL-treated CNF (after removal of IL).

	Glucose (%)	Xylose (%)	Mannose (%)	Crystallinity (%)	Crystalline type
Initial CNF	63.1	22.2	0.4	58	Cellulose I
CNF15	69.3	24.5	0.4	59	Cellulose I
CNF50	66.5	23.7	0.4	55	Cellulose I

Table S2. Nomenclature and concentrations of all components in suspensions and corresponding nanopaper.

Suspension code	Dispersant	IL concentration (wt. %)	CNF concentration (wt. %)	Nanopaper code
Starting CNF batch	water	0	0.4	CNF
0.34%CNF-5%IL-W	IL-water	5	0.34	CNF5
0.28%CNF-15%IL-W	IL-water	15	0.28	CNF15
0.16%CNF-30%IL-W	IL-water	30	0.16	CNF30
0.15%CNF-50%IL-W	IL-water	50	0.15	CNF50
0.34%CNF-5%water	water	0	0.34	-
0.28%CNF-15%water	water	0	0.28	-
0.16%CNF-30%water	water	0	0.16	-

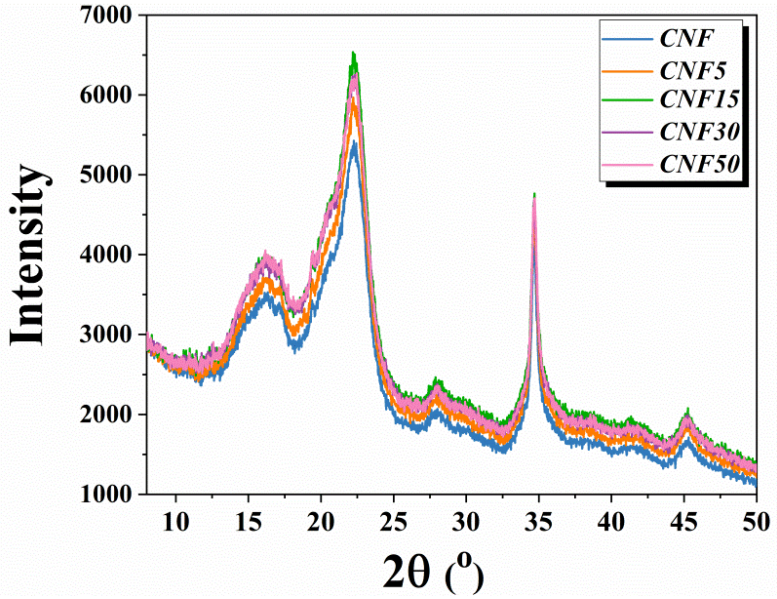

Figure S2. XRD profiles of nanopapers from 0.4 wt.% CNF-water ("CNF") and CNF-IL-water suspensions.

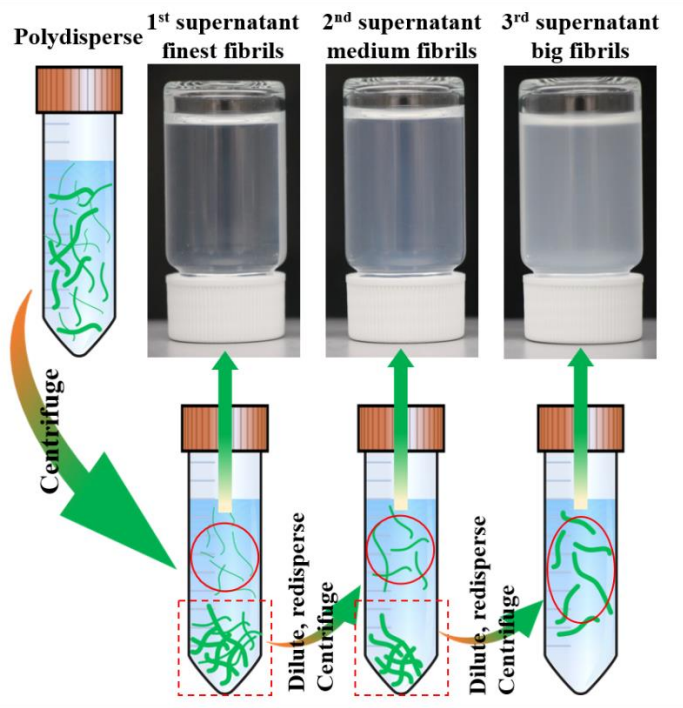

Figure S3. Schematic illustration of CNF fractionation by successive centrifugation. The three resulting fractioned CNF suspensions have an equal concentration of 0.06 wt. % after dilution with water.

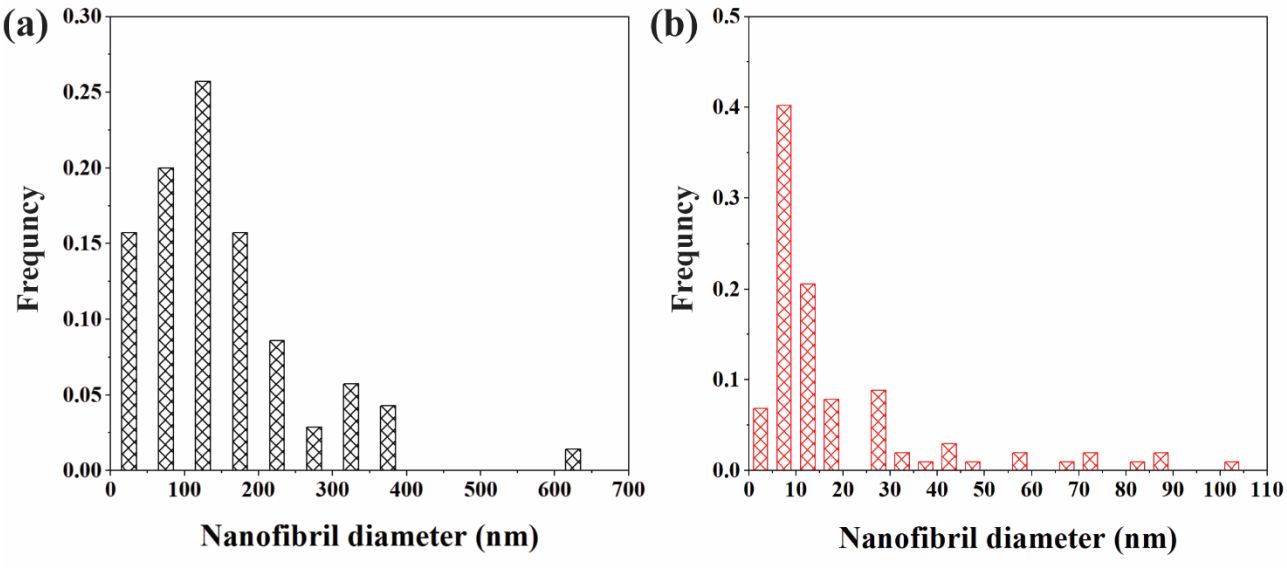

Figure S4. Cryo-TEM based CNF diameter distributions before (a) and after (b) the treatment with IL.

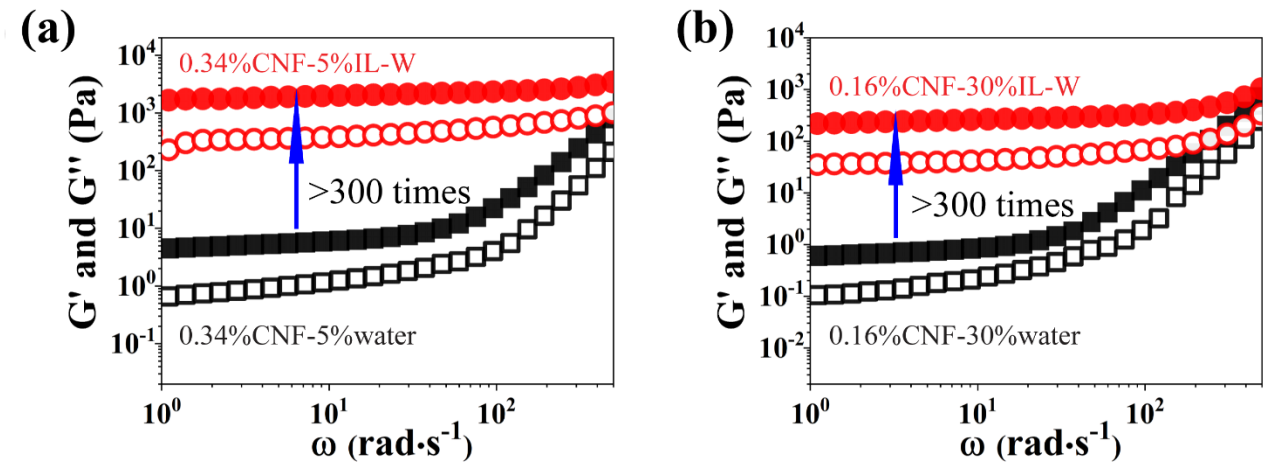

Figure S5. Viscous (open symbols) and elastic (filled symbols) moduli of CNF suspension in water (black symbols) and in IL-water (red symbols): a) of 0.34 wt. % CNF dispersed in water and in 5%IL-water, and b) of 0.16 wt. % CNF dispersed in water and in 30%IL-water.

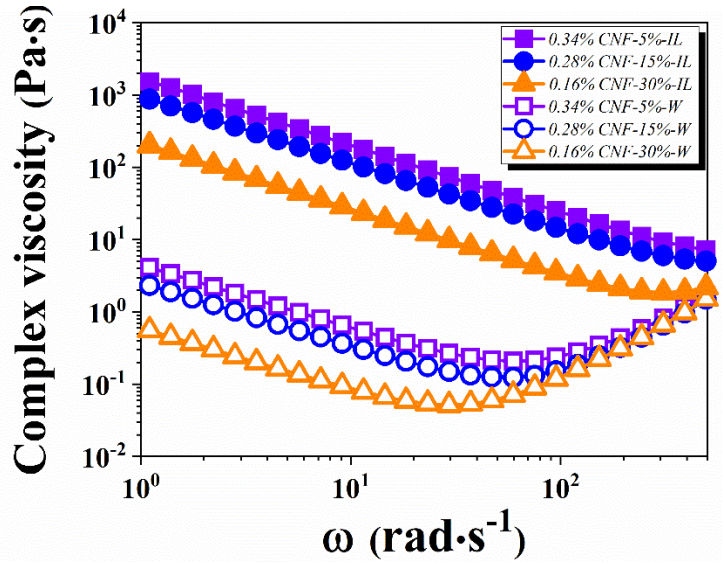

Figure S6. Complex viscosity as a function of frequency of CNF suspension in water (open symbols) and in the corresponding IL-water (filled symbols).

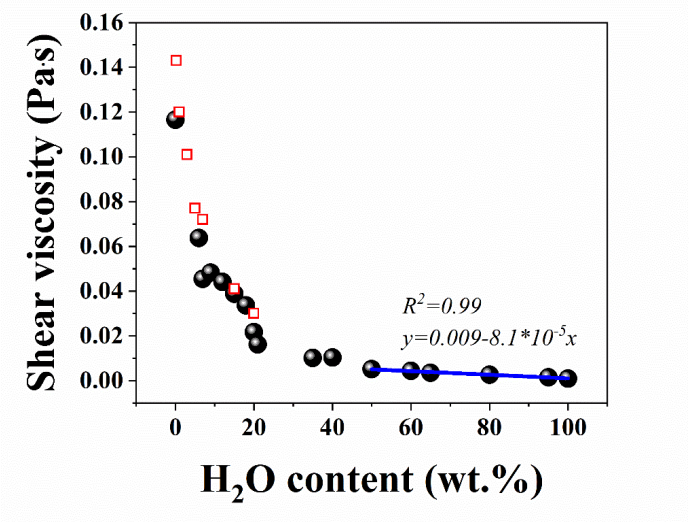

Figure S7. Shear viscosity of [EMIM[[OAc]-water mixture as a function of water content, at 25 °C. Filled points are data taken from ref. 1 and open points are this work showing very good reproducibility. It was demonstrated that [EMIM][OAc]-water mixtures are Newtonian liquids at all mixture compositions.[1] Solid line is a linear approximation for high water content IL-water mixtures used in this work.

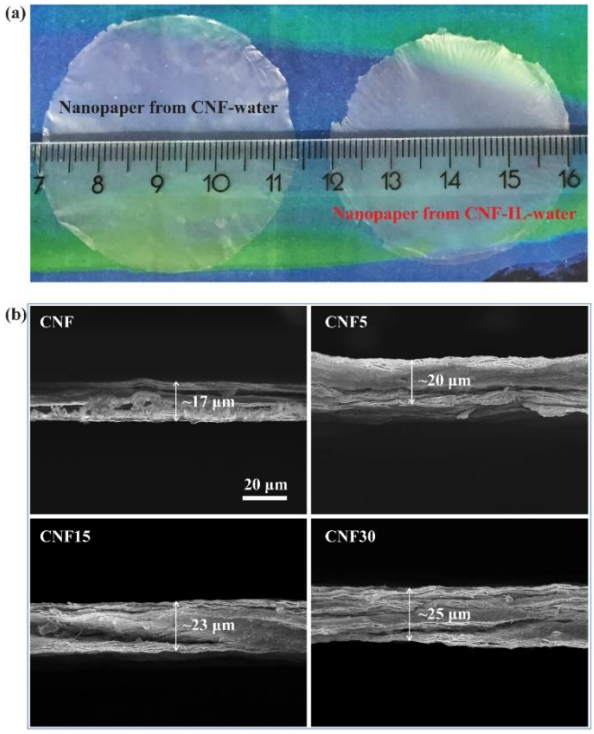

Figure S8. (a) Photos illustrating nanopaper shrinkage in longitudinal direction and (b) SEM images of cryo-fractured nanopaper in the transversal direction (the scale of 20 µm is the same for all images).

Table S3. Physical and mechanical properties of nanopapers from CNF-water and CNF-IL-water suspensions of different IL concentration. Optical properties are reported at wavelength of 550 nm.

	CNF	CNF5	CNF15	CNF30
Crystallinity (%)	58	59	59	57
Density (g/cm^3)	1.26±0.02	1.11±0.06	0.99±0.04	1.02±0.04
Porosity (%)	13.3±1.1	24.2±3.9	32.5±2.5	29.8±2.9
Transmittance (%)	86.7	86.2	86.2	85.2
Haze (%)	44.9	46.5	47.5	51.5
Ra (nm)	89±20	77±12	84 ± 17	79±15
Rq (nm)	110±23	95±15	102±20	97±18
Strength at break (MPa)	96.3±4.9	174.2±13.4	233.3±28.4	178.7±17.2
Young's modulus (GPa)	3.4±0.8	2.3±0.1	2.3±0.1	2.7±0.1
Strain at break (%)	7.5±1.3	19±4.5	29.4±5.3	17.6±1.1
Work of fracture (MJ/m^3)	4.9±0.7	18.2±2.9	38.1±13.1	17.9±2.3
Specific modulus ($GPa/(g/cm^3)$)	2.7±0.6	2.1±0.1	2.3±0.1	2.6±0.1

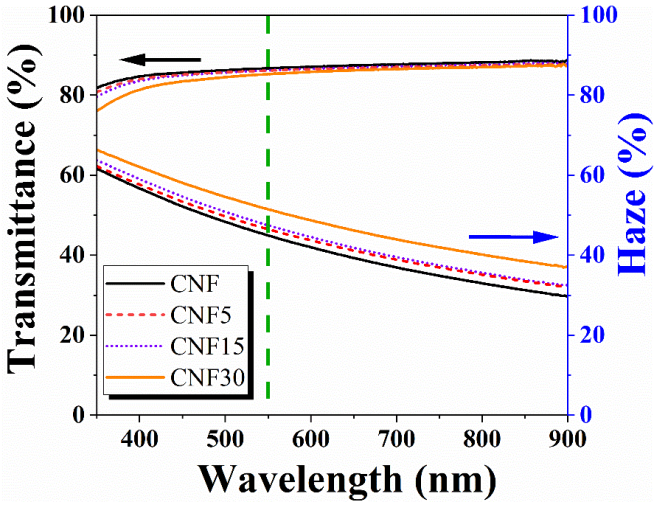

Figure S9. Optical transmittance and haze of nanopapers from CNF-water and CNF-IL-water suspensions.

Table S4. Mechanical properties of nanopapers shown on the Ashby plot in Figure 4. CLP= Colloidal lignin particles, VP= Vitrimer nanoparticles, HEC= Hydroxyethylcellulose, THA^+= Tetrahexyl ammonium.

No.	Materials	Strain (%)	Toughness (MJ/m^3)	Strength (MPa)	Modulus (GPa)	Density (g/cm^3)	Ref.
1	CNF	9.4±2.3	8.2±2.4	132±14.8	5.7±1.2	0.92±0.21	[2]
2	TEMPO-CNF (11 nm)	8.5±0.5	16.9±0.1	275.2±25	-	1.2	[3]
3	Enzymatic-CNF	10.1±1.4	15.1±1.9	214±6.8	13.2±0.6	1.08	[4]
4	Bacterial cellulose	7.5±0.6	5.8±0.6	123±7	12±1.1	0.72±0.02	[5]
5	Delignified wood	4	7.38	350	-	-	[6]
6	CNF/10%CLP	16.6±1.9	16±2.7	159.7±16.1	5.6±0.3	1.07±0.06	[2]
7	TEMPO-CNF/50%VP	19±1	4.2±0.3	28±1	1.2±0.2	-	[7]
8	CNF-IL welded	11.7±1.4	20±3	265±13	6.2±0.6	-	[8]
9	31%CNF/HEC56%	24.4±2.6	27.1±4.1	147±6	4.58±0.45	1.20±0.11	[9]
10	TEMPO-CNF- THA^+	21±2	38±5	272±10	16±1	1.41±0.03	[10]
11	CNF15	29.4±5.3	38.1±13.1	233.3±28.4	2.3±0.1	0.99±0.04	this work

References

(1) Hall C. A.; Le K. A.; Rudaz C.; Radhi A.; Lovell C. S.; Damion R. A.; Budtova T.; Ries M. E. Macroscopic and Microscopic Study of 1-Ethyl-3-Methyl-Imidazolium Acetate-Water Mixtures. *J. Phys. Chem. B* **2012**, *116*, 12810-8.

(2) Farooq, M.; Zou, T.; Riviere, G.; Sipponen, M. H.; Österberg, M. Strong, Ductile, and Waterproof Cellulose Nanofibril Composite Films with Colloidal Lignin Particles. *Biomacromolecules* **2019**, *20*, 693-704.

(3) Zhu, H.; Zhu, S.; Jia, Z.; Parvinian, S.; Li, Y.; Vaaland, O.; Hu, L.; Li, T. Anomalous Scaling Law of Strength and Toughness of Cellulose Nanopaper. *Proc. Natl. Acad. Sci. U S A* **2015**, *112*, 89718976.

(4) Henriksson, M.; Berglund, L. A.; Isaksson, P.; Lindstrom, T; Nishino, T. Cellulose Nanopaper Structures of High Toughness. *Biomacromolecules* **2008**, *9*, 1579-1585.

(5) Lee, K. Y.; Tammelin, T.; Schulfter, K.; Kiiskinen, H.; Samela, J.; Bismarck, A. High Performance Cellulose Nanocomposites: Comparing the Reinforcing Ability of Bacterial Cellulose and Nanofibrillated Cellulose. *ACS Appl. Mater. Interfaces* **2012**, *4*, 4078-4086.

(6) Zhu, M.; Wang, Y.; Zhu, S.; Xu, L.; Jia, C.; Dai, J.; Song, J.; Yao, Y.; Wang, Y.; Li, Y.; Henderson, D. Anisotropic, Transparent Films with Aligned Cellulose Nanofibers. *Adv. Mater.* **2017**, *29*, 1606248.

(7) Lossada, F.; Guo, J.; Jiao, D.; Groeer, S.; Bourgeat-Lami, E.; Montarnal, D.; Walther, A. Vitrimer Chemistry Meets Cellulose Nanofibrils: Bioinspired Nanopapers with High Water Resistance and Strong Adhesion. A. Walther, *Biomacromolecules* **2019**, *20*, 1045-1055.

(8) Reyes, G.; Borghei, M.; King, A. W.; Lahti, J.; Rojas, O. J. Solvent Welding and Imprinting Cellulose Nanofiber Films Using Ionic Liquids. *Biomacromolecules* **2019**, *20*, 502-514.

(9) Sehaqui, H.; Zhou, Q.; Berglund, L. A. Nanostructured Biocomposites of High Toughness—A Wood Cellulose Nanofiber Network in Ductile Hydroxyethylcellulose Matrix. *Soft Matter* **2011**, *7*, 7342-7350.

(10) Benítez, A. J.; Walther, A. Counterion Size and Nature Control Structural and Mechanical Response in Cellulose Nanofibril Nanopapers. *Biomacromolecules* **2017**, *18*, 1642-1653.